Carbon Efficiency Comparison of FRP and Steel Bars for Reducing the Embodied Carbon of Concrete Structural Elements

Shizhe Hong [a,*], John Orr [b], Arnaud Delaplace [a]

[a] Holcim Innovation Center, Saint-Quentin Fallavier, France

[b] University of Cambridge, Cambridge, UK

Abstract

In recent years, FRP (Fibre-Reinforced Polymer) bars have been considered to be a promising alternative to conventional steel bars for reducing the CO_2 emissions of concrete structural elements, whilst their environmental performance compared to traditional steel bars requires quantitative assessment. This paper introduces a multi-level comparative framework to evaluate the carbon efficiency of FRP bars compared to steel bars, from the material level to the section level and structural element levels, leading to quantitative comparative outcomes useful for decision-making when selecting the most carbon-efficient rebar type for achieving the lowest embodied carbon (cradle-to-gate) of structural elements. Each comparison level has its applicability depending on the specific context of construction projects. Because relative environmental performance can vary significantly in function of material and environmental data, the developed comparative framework aims to provide the rigorous methodology to follow, which can be adapted to any construction project by updating material and environmental datasets, rather than declaring a universally superior rebar type. Steel and BFRP (basalt FRP) bars are compared, based on the assumed material and environmental data, as an example to demonstrate how to apply the proposed comparative formwork. Results indicate that the optimal solution depends mainly on the structural parameters (such as span and slab thickness) as well as the assumed carbon data. For prismatic elements, the optimal choice between steel and BFRP bar is strongly influenced by the selection of slab thickness. For non-prismatic elements, it is found that non-prismatic BFRP-reinforced slabs have 4.8%–14.4% lower CO_2 than non-prismatic steel-reinforced slabs and can save up to 63% of CO_2 compared to the traditional solution (prismatic steel-reinforced slabs) in the presented examples.

Keywords: FRP (Fibre-Reinforced Polymer), CO_2, reinforcement, concrete structure

***** Corresponding author.

E-mail addresses: s.hong@holcim.com (S. Hong), jjo33@cam.ac.uk (J. Orr), arnaud.delaplace@holcim.com (A. Delaplace)

1. Introduction

FRP materials were firstly investigated as the reinforcement of concrete for the construction of highways in the United States during the 1950s, because the deicing salts, often used on highway bridges, can exacerbate the corrosion problem of steel reinforcement but do not have such impact on FRP reinforcement [1]. There exist mainly four types of FRP reinforcement classified by the type of fibre: carbon (CFRP), glass (GFRP), basalt (BFRP) and aramid (AFRP). They can be used as internal reinforcement in concrete elements, such as slabs [2], [3] and beams [4], typically in the form of bars or grids, or applied as external reinforcement for retrofit, typically in the form of plates or sheets [5]. Compared to steel reinforcement, FRP reinforcement has many advantages, such as their higher tensile strength, lighter weight (around 1/4 of steel), higher resistance to the corrosion induced by chloride ions, electrical non-conductivity, and lower thermal conductivity [1], [6]. However, some drawbacks have limited the wider usage of FRP as the reinforcement for concrete, including its lower elastic modulus than steel (making FRP-reinforced elements more prone to excessive deformation), low ductility (almost linear behaviour till rather brittle failure) [7] and higher price (mainly for most CFRP and AFRP) than steel.

As the CO_2 reduction is becoming an increasingly urgent issue today, a rethink of FRP reinforcement attracts more interest, and its potential as an alternative to replace traditional steel reinforcement to reduce CO_2 emissions [8] is worth investigating. Many researchers compared the CO_2 emissions of FRP-reinforced concrete elements with their steel-reinforced counterparts and argued that FRP reinforcement can provide opportunities for reducing the CO_2 emissions of reinforced-concrete structural elements.

N. Stoiber et al. [9] conducted a cradle-to-gate life cycle assessment of CFRP reinforcement (modules A1–A3, which correspond to the product stage), and found that CFRP reinforcement has better environmental performance than steel reinforcement when its high tensile strength and low density are taken into count by comparing the Global Warming Potential (GWP) per MPa (characteristic tensile strength for CFRP, yield strength for steel) as well as per density unit. A. Pavlović et al. [10] compared the GWP (A1–A3) of identically sized bars (1 m long, 6 mm diameter) made from different materials and found that the GWP of the BFRP bar was 75% lower than that of unrecycled steel and 24% lower than that of recycled steel (electric arc furnace process); they also conducted the comparison at the structural element level taking the load-bearing capacity at the serviceability limit state (SLS) deflection limit of span/250 as the structural equivalence, and found that the GWP (modules A1–A5, corresponding to the product and construction stages) of the studied BFRP-reinforced beam is 7% lower than its steel-reinforced counterpart. N. Garg and

S. Shrivastava [11] compared the CO_2 emissions (modules A1–A3) per M_u (ultimate moment bearing capacity) of FRP- and steel-reinforced 2.75 m long beams, and found that CFRP-, BFRP- and GFRP-reinforced beams can save 39%–43% of CO_2 emissions compared with steel-reinforced beams. Other researchers found environmental benefits of using FRP reinforcement in other structures, such as bridges [12] and facade panels [13]. Although previous studies made meaningful comparisons, some limitations restrict the generality of the conclusions: (1) Some comparisons only at the material level cannot well represent the carbon efficiency of the structural elements because of ignoring the complexity of the relationship between the material properties and the design of structural elements; (2) For comparisons at the material level, a reasonable mechanical equivalence, taking into account the differences in density, should be maintained when comparing different solutions; (3) For comparisons at the structural element level, ULS-based comparisons alone could not lead to conclusions with wide applicability because the design of FRP-reinforced structural elements is often governed by SLS criteria; (4) For both comparisons at the material level and structural element level, the differences between steel and FRP reinforcement in terms of various reduction factors for safety considerations were not taken into account.

Therefore, the following research questions need to be addressed: How can reinforcing bar selection (steel vs. FRP) be systematically evaluated to achieve the minimum embodied carbon in concrete structural elements while accounting for material (strength, stiffness and density), structural design (ULS and SLS), and code-level constraints (such as reduction factors)? How can the comparison method be unified to ensure inter-study comparability and eliminate methodological bias in future comparisons for construction projects?

To bridge this gap, this paper will introduce a comparative framework for multi-level comparisons of the carbon efficiency between FRP and steel bars for reinforcing concrete, allowing decision making when selecting the optimal rebar type for reducing the embodied carbon of structural elements.

2. Methodology and scope

2.1. Multi-level comparison

This paper introduces a framework for comparisons at different levels, as shown in Table 1. The scope of this framework is limited to FRP reinforcing bars used as internal reinforcement in concrete and does not cover prestressed tendons or externally bonded reinforcement systems (such as FRP plates or sheets).

At the preliminary design stage when the carbon data of locally available reinforcement are accessible but detailed information regarding the structural configuration remains unknown, the carbon efficiency assessment at the material level can serve as an effective basis for quick comparison, although the resulting conclusions are necessarily approximate.

When section-level information becomes available, which means the section size is already determined and the requirements for strength and stiffness can be established through analysis, the comparison of carbon efficiency at the section level can provide more precise conclusions, taking into account the section-specific data.

When detailed structural information (such as span and maximum section depth) is available and the structural elements possess a constant prismatic section along the span, the carbon efficiency comparison at the prismatic structural element level can be conducted, enabling a more accurate estimation of material quantities and carbon emissions based on specific structural characteristics.

Finally, when detailed data are also available but the structural elements can be non-prismatic (which means the sectional dimensions can vary along the span), the assessment at the non-prismatic structural element level can be performed, allowing for a more comprehensive and precise analysis of carbon efficiency, capturing the effects of geometric variability and shape optimisation on these structural elements.

Table 1. Multi-level comparison of carbon efficiency of FRP and steel reinforcing bars

<table>
<tr><th>Level of comparison</th><th colspan="2">Description</th></tr>
<tr><td>Material level</td><td colspan="2">Material-level comparison taking the strength and the stiffness of the material as the equivalence and considering the influence of various reduction factors of the design process</td></tr>
<tr><td>Section level</td><td colspan="2">Section-level comparison taking the strength and stiffness of the section as the equivalence to find the optimal choice of bars for reinforcing a given section</td></tr>
<tr><td>Prismatic structural element level</td><td rowspan="2">Structural-element-level comparison, taking into account both ULS and SLS criteria</td><td>Assuming the elements are prismatic</td></tr>
<tr><td>Non-prismatic structural element level</td><td>Assuming the elements can be non-prismatic</td></tr>
</table>

2.2. Influence of the differences in safety factors and designs methods

When comparing steel and FRP bars for reinforcing concrete structures, many differences beyond their strength and stiffness can significantly influence the quantity of reinforcement in structural designs using different reinforcing bars. These differences should be taken into account when comparing their carbon efficiency.

(1) More severe strength reduction factors for bending failure of FRP-reinforced elements

FRP-reinforced elements in flexure exhibit linear behaviour until failure. Two types of failure can happen: compression-controlled failure (by concrete crushing) and tension-controlled failure (by FRP rupture). The tension-controlled failure is rather sudden and not preferred. To achieve the same target reliability level, smaller strength reduction factors for flexure failure (which means the strength is reduced more) are required for FRP-reinforced elements than for their steel-reinforced counterparts.

For example, the American code ACI 318-19 [14] applies a strength reduction factor of 0.90 for steel-reinforced sections in flexure with tension-controlled failure, whilst ACI 440-1R [1] applies a strength reduction factor between 0.55 and 0.65 for FRP-reinforced sections in flexure depending on the failure mode.

(2) Less time-dependent deflection increase for FRP-reinforced elements

The time-dependant deflection increase of FRP-reinforced elements is less than that of steel-reinforced elements [15]. The American code ACI 440-1R [1] for FRP-reinforced concrete elements adopts the same form of relationship between short-term and long-term deflection as the one adopted in ACI 318-19 [14] for steel-reinforced concrete elements, but multiplies the long-term deflection result by 0.6 for FRP-reinforced elements.

(3) Creep rupture of FRP bars

FRP bars subjected to a constant tension after a specific period of time (depending on the stress level) can suddenly fail, called “creep rupture” [16]. To avoid this, ACI 440-1R [1] limits the stress level of the bars under unfactored sustained loads to 0.2, 0.3, and 0.5 of the design tensile strength, for GFRP, AFRP, and CFRP, respectively. The French AFGC recommendation [17] recommends a ratio of 0.25 for BFRP and GFRP, 0.4 for AFRP and 0.6 for CFRP as the stress limit under the quasi-permanent load combination.

(4) Durability of FRP bars

The tensile strength of FRP bars decreases with time due to long-term exposure to the environment; therefore ACI 440-1R [1] applies an environmental reduction factor, whose value varies between 0.8 and 1.0 depending on the exposure conditions and the type of FRP.

The current version of Eurocode 2 [18] does not include design provisions for FRP-reinforced concrete elements. While American code ACI 440-1R [1] covers CFRP, GFRP, and AFRP reinforcing bars, it does not explicitly include BFRP bars. The French AFGC recommendation [17] encompasses all four types of FRP bar. When comparing the CO_2 emissions of steel- and FRP-reinforced elements, it is highly recommended to adhere to the same design code or at least design codes within the same family. Distinct code families may apply different methodologies, safety concepts and provisions to ensure structural reliability [19], leading to difficulties in straightforward comparisons between steel and FRP. Nevertheless, it is worth noting that this study aims to develop a comparison framework which is general and applicable across all four FRP bar types regardless of the selection of the governing design code, as the underlying methodology remains consistent.

2.3. Carbon data

The "carbon emissions" or "CO_2 emissions" mentioned in this paper relate to the GWP from cradle to gate (stages A1–A3). As shown in Table 2, the comparison examples involve three groups of carbon factors for steel bars and FRP bars: high, medium and low CO_2 groups, which represent, respectively, the upper bound, the representative mid-range value and the lower bound of the GWP. The carbon factors for concrete used in this paper for the comparison examples are shown in Table 3.

Unlike steel bars which benefit from extensive academic literature, abundant environmental datasets, and numerous industrial Environmental Product Declarations (EPDs), available life cycle inventory data for BFRP bars remains severely limited. M. Inman et al. [20] reported that the GWP (A1–A3) of BFRP bars range from 1.67 to 2.98 $kgCO_2eq/kg$ as the resin content increases from 20% to 40%. Similarly, A. Pavlović et al. [10] observed values of GWP(A1–A3) of BFRP bars between 2.71 and 3.20 $kgCO_2eq/kg$ when the weight percentage of basalt fiber varies from 70% to 85%. Three industrial EPDs [21], [22], [23] indicate consistent values between 2.69 and 3.14 $kgCO_2eq/kg$. Based on the synthesized data, the central estimate is established at 2.85 $kgCO_2eq/kg$. Upper- and lower-bound scenarios are defined as 3.20 and 2.50 $kgCO_2eq/kg$, which reflect a symmetric ±12% variation relative to the baseline.

Whether for concrete, steel bars or FRP bars, the carbon data can differ significantly depending on the country, region, manufacturing process, recycling ratio, transport distance and other factors. When the carbon data change, the carbon efficiency comparison results can vary significantly. This paper aims at introducing a comparative framework for comparisons at different levels, and the examples presented in this paper, using the assumed carbon data, serve solely to demonstrate how to apply the proposed methods. With the introduced comparative multi-level framework and methods, comparisons can be conducted on a case-by-case basis with locally available materials, real project information and updated carbon data.

Table 2. Carbon factors used for reinforcement in the example of comparison between steel and BFRP bars

Group	Steel		BFRP	
	GWP (A1–A3), in $kgCO_2eq/kg$	Sources	GWP (A1–A3), in $kgCO_2eq/kg$	Sources
High-CO_2	3.95	[24], [25] (Basic Oxygen Furnace production)	3.20	Hypothesised values based on the research [10], [20] and industrial EPDs [21], [22], [23]
Medium-CO_2	1.96	[24], [26] (typical average value)	2.85	
Low-CO_2	0.79	[24], [27] (Electric Arc Furnace production)	2.50	

Table 3. Carbon factors used for concrete (C25/30) in the example of comparison between steel and BFRP bars

Type of C25/30 concrete	GWP (A1–A3), in $kgCO_2eq/m^3$	Sources
Ordinary	309	[28] (average of Band F, GCCA definition)
Low-CO_2	170	[29]
Ultra-low-CO_2	49	[28], [29] (average of Band A, GCCA definition)

3. Carbon efficiency comparison at the material level

This section will introduce the comparison of carbon efficiency at the material level, which is convenient for a quick comparison when more architectural and structural information is not yet available at an early stage of a construction project.

The carbon efficiency of FRP or steel reinforcing bars can be expressed as:

$$\frac{1}{e} = \frac{c\rho}{\prod_{i=1}^{n} \alpha_i \cdot P} \quad \text{(Eq. 1)}$$

where e is the carbon efficiency (the reciprocal of the GWP that has to be created to achieve the equivalent strength or stiffness), c is the carbon factor (A1–A3, in $kgCO_2eq/kg$), ρ is the density (in kg/m^3), P is the material property (either strength in MPa, or stiffness in GPa), and α_i is the ith of n reduction factors applied to the considered material property.

The ratios of carbon efficiency of FRP to steel reinforcing bars can be obtained as:

$$\frac{e_{\text{f, strength}}}{e_{\text{s, strength}}} = \frac{\prod_{i=1}^{n_{\text{f, strength}}} \alpha_{\text{f, strength, } i}}{\prod_{i=1}^{n_{\text{s, strength}}} \alpha_{\text{s, strength, } i}} \cdot \left(\frac{c_{\text{f}}}{c_{\text{s}}}\right)^{-1} \cdot \left(\frac{\rho_{\text{f}}}{\rho_{\text{s}}}\right)^{-1} \cdot \frac{f_{\text{f}}}{f_{\text{s}}} \qquad \text{(Eq. 2a)}$$

$$\frac{e_{\text{f, stiffness}}}{e_{\text{s, stiffness}}} = \frac{\prod_{i=1}^{n_{\text{f, stiffness}}} \alpha_{\text{f, stiffness, } i}}{\prod_{i=1}^{n_{\text{s, stiffness}}} \alpha_{\text{s, stiffness, } i}} \cdot \left(\frac{c_{\text{f}}}{c_{\text{s}}}\right)^{-1} \cdot \left(\frac{\rho_{\text{f}}}{\rho_{\text{s}}}\right)^{-1} \cdot \frac{E_{\text{f}}}{E_{\text{s}}} \qquad \text{(Eq. 2b)}$$

where the subscripts f and s denote FRP and steel bars, respectively; $e_{\text{f, strength}}$ and $e_{\text{s, strength}}$ are the carbon efficiencies for strength; $e_{\text{f, stiffness}}$ and $e_{\text{s, stiffness}}$ are the carbon efficiencies for stiffness; f_{f} and f_{s} are the strengths; E_{f} and E_{s} are the elastic moduli; $\alpha_{\text{f, strength, } i}$, $\alpha_{\text{s, strength, } i}$, $\alpha_{\text{f, stiffness, } i}$ and $\alpha_{\text{s, stiffness, } i}$ are the ith reduction factors applied to the strength or stiffness; $n_{\text{f, strength}}$, $n_{\text{s, strength}}$, $n_{\text{f, stiffness}}$ and $n_{\text{s, stiffness}}$ are the numbers of various reduction factors to take into account; c_{f} and c_{s} are the carbon factors; ρ_{f} and ρ_{s} are the densities.

Table 4. Comparison of the carbon efficiency of steel and BFRP bars at the material level

Type of bars	Carbon factor ($kgCO_2$ eq/kg)	Density (kg/m^3)	Comparison for strength			Comparison for stiffness		
			Strength[a] (MPa)	Reduction factors[b] (ACI codes [1], [14])	$\frac{e_{\text{f, strength}}}{e_{\text{s, strength}}}$ (Eq. 2a)	Elastic modulus (GPa)	Reduction factors	$\frac{e_{\text{f, stiffness}}}{e_{\text{s, stiffness}}}$ (Eq. 2b)
BFRP	2.85	2000	1200	Φ = 0.6[c] C_E = 0.8	4.11	50	-	0.67
Steel	1.96	7850	420[d]	Φ = 0.9		200	-	

(Notes: [a] Specified yield strength for steel bars; guaranteed tensile strength for FRP bars.

[b] ϕ: strength reduction factor; C_E: environmental reduction factor of FRP bars. The simplifying assumption is made that the strength reduction factors are applied directly to the strengths.

[c] The strength reduction factor is between 0.55 and 0.65 depending on the failure mode; a value of 0.6 is assumed here.

[d] ASTM A615 Grade 60 bars [30].)

Table 4 shows an example of carbon efficiency comparison between steel and BFRP bars at the material level, using the ACI family of codes (ACI 440-1R [1] for FRP bars and ACI 318-19 [14] for steel bars). The results show that the carbon efficiency of BFRP bars is approximately 4 times that of steel bars for strength, whilst 0.67 time that of steel bars for stiffness.

This seems to suggest using BFRP bars when ULS criteria would govern the design whilst using steel bars when excessive deformation would govern the design. However, whether ULS or SLS criteria govern the design can be determined not before, but after, the type of bar is chosen. Additionally, the comparison at the material level does not reflect the influence of section- and structural-element-level factors on the CO_2 emissions. Therefore, a comparison at the material level can serve as a quick, simplified comparison, whilst comparisons at the section and structural element levels are needed to provide further insight and more precise results.

4. Carbon efficiency comparison at the section level

Reinforcing bars can provide the strength and stiffness required for a section to satisfy the ULS and SLS criteria, respectively. To determine the carbon-optimal rebar type solution among steel-only, FRP-only, and hybrid steel-FRP solutions (the strain compatibility and structural feasibility of which are well-established [31], [32], [33], [34]), the problem can be formulated as an optimisation problem.

Supposing that a section in a structural element in flexure is reinforced with a combination of steel and FRP bars to satisfy ULS and SLS requirements, and the reinforcement solution is denoted as $(A_\mathrm{s}, A_\mathrm{f})$ where A_s and A_f are the reinforcement areas of steel and BFRP bars, respectively; the needed strength for this section, characterised by the product of tensile strength and cross-sectional area of the reinforcement ($f_\mathrm{s}A_\mathrm{s}$ or $f_\mathrm{f}A_\mathrm{f}$), should be no less than the required strength threshold T_1 (in MPa·m^2); and the needed stiffness for the section, characterised by the product of elastic modulus and cross-sectional area of the reinforcement, should be no less than the required stiffness threshold T_2 (in GPa·m^2). The values of T_1 and T_2 can be predetermined through sectional strength analysis and deflection control analysis, respectively. With the aim of minimising the embodied carbon of the reinforcement $C = c_\mathrm{s}\rho_\mathrm{s}A_\mathrm{s} + c_\mathrm{f}\rho_\mathrm{f}A_\mathrm{f}$, the optimisation problem can be posed as:

Find the optimal $\mathbf{\Omega}^* = (A_\mathrm{s}, A_\mathrm{f})^*$ in the set $\mathbf{\Omega}_\mathrm{admissible}$ such that:

$$C[(A_\mathrm{s}, A_\mathrm{f})^*] = \min_{\mathbf{\Omega}} C[(A_\mathrm{s}, A_\mathrm{f})] \quad \text{(Eq. 3a)}$$

where:

$$C = c_\mathrm{s}\rho_\mathrm{s}A_\mathrm{s} + c_\mathrm{f}\rho_\mathrm{f}A_\mathrm{f} \quad \text{(Eq. 3b)}$$

with the constraints that

$$\begin{cases} f_\mathrm{s}A_\mathrm{s} + f_\mathrm{f}A_\mathrm{f} \geq T_1 \\ E_\mathrm{s}A_\mathrm{s} + E_\mathrm{f}A_\mathrm{f} \geq T_2 \end{cases} \quad \text{(Eq. 3c)}$$

(Eq. 3d)

By formulating this optimisation problem, the functional unit is established as the reinforcement areas $(A_\mathrm{s}, A_\mathrm{f})$ that can provide required strength T_1 and stiffness T_2 for a section.

The constraints of Eqs. 3c and 3d can be illustrated as shown in Fig. 1. The point $(A_\mathrm{s}, A_\mathrm{f})$ represents the reinforcing area of the section. To satisfy the constraints, the reinforcement solution $(A_\mathrm{s}, A_\mathrm{f})$ should be located in the feasible half-space shown in Fig. 1a for strength and of Fig. 1b for stiffness.

As shown in Fig. 2, for the point $(A_\mathrm{s}, A_\mathrm{f})$ located in the feasible domain, the line for Eq. 3b intersects the vertical axis and the intercept is $C/(c_\mathrm{f}\rho_\mathrm{f})$. When the point $(A_\mathrm{s}, A_\mathrm{f})$ moves in the feasible domain, the line for Eq. 3b moves while maintaining a constant slope of $-c_\mathrm{s}\rho_\mathrm{s}/(c_\mathrm{f}\rho_\mathrm{f})$. Finding $\min_{\boldsymbol{\Omega}} C[(A_\mathrm{s}, A_\mathrm{f})]$ is transformed into finding the minimum intercept of the line for Eq. 3b on the vertical axis.

The location of the optimal point $(A_\mathrm{s}, A_\mathrm{f})$ depends on the relative positions of the three lines (Fig. 1a, Fig. 1b and Fig. 2) as well as their respective slope (denoted k_1, k_2, and k_3, respectively). As $|k_1| = f_\mathrm{s}/f_\mathrm{f}$ which is usually less than 1 and $|k_2| = E_\mathrm{s}/E_\mathrm{f}$ is usually much larger than 1, it can be assumed that $|k_1| < |k_2|$. However, the relationship between $|k_3| = c_\mathrm{s}\rho_\mathrm{s}/c_\mathrm{f}\rho_\mathrm{f}$ and the other two slopes is uncertain since there is substantial uncertainty in the carbon data, which may vary considerably depending on the fabrication process, country, transport distance, and other parameters.

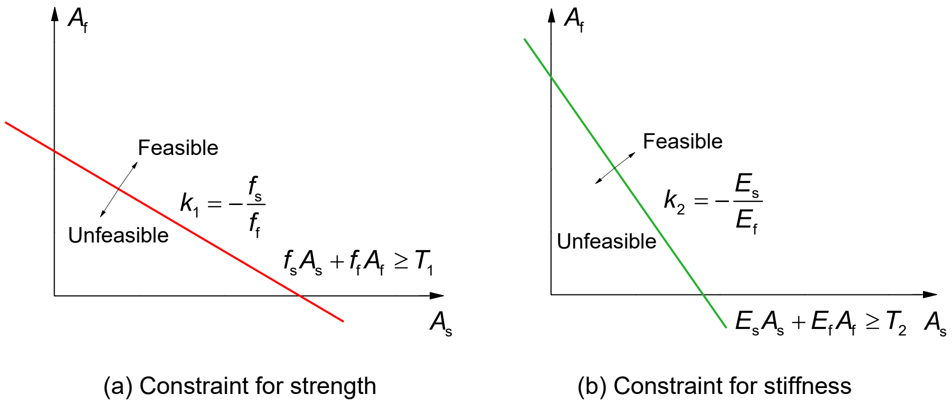

Fig. 1. Constraints of the optimization problem defined by Eqs. 3c and 3d

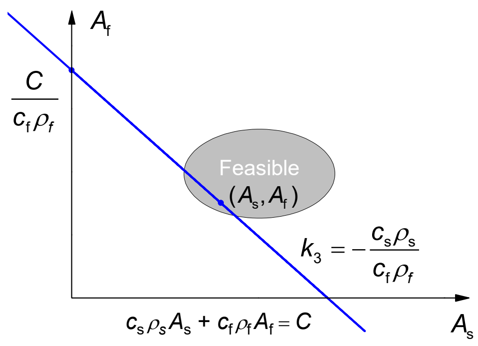

Fig. 2. Solutions in the feasible domain and their carbon emissions (Eq. 3b)

Therefore, different cases may arise, as shown in Fig. 3, and the physical meaning of each case is explained in Table 5. The optimal solution is: using steel bars in Cases 1b, 2b and 3a; using FRP bars in Cases 1a, 2a and 3e; using the steel-FRP hybrid solution in Cases 1c, 2c and 3b, 3c and 3d. The physical meaning of each case is given in Table 5.

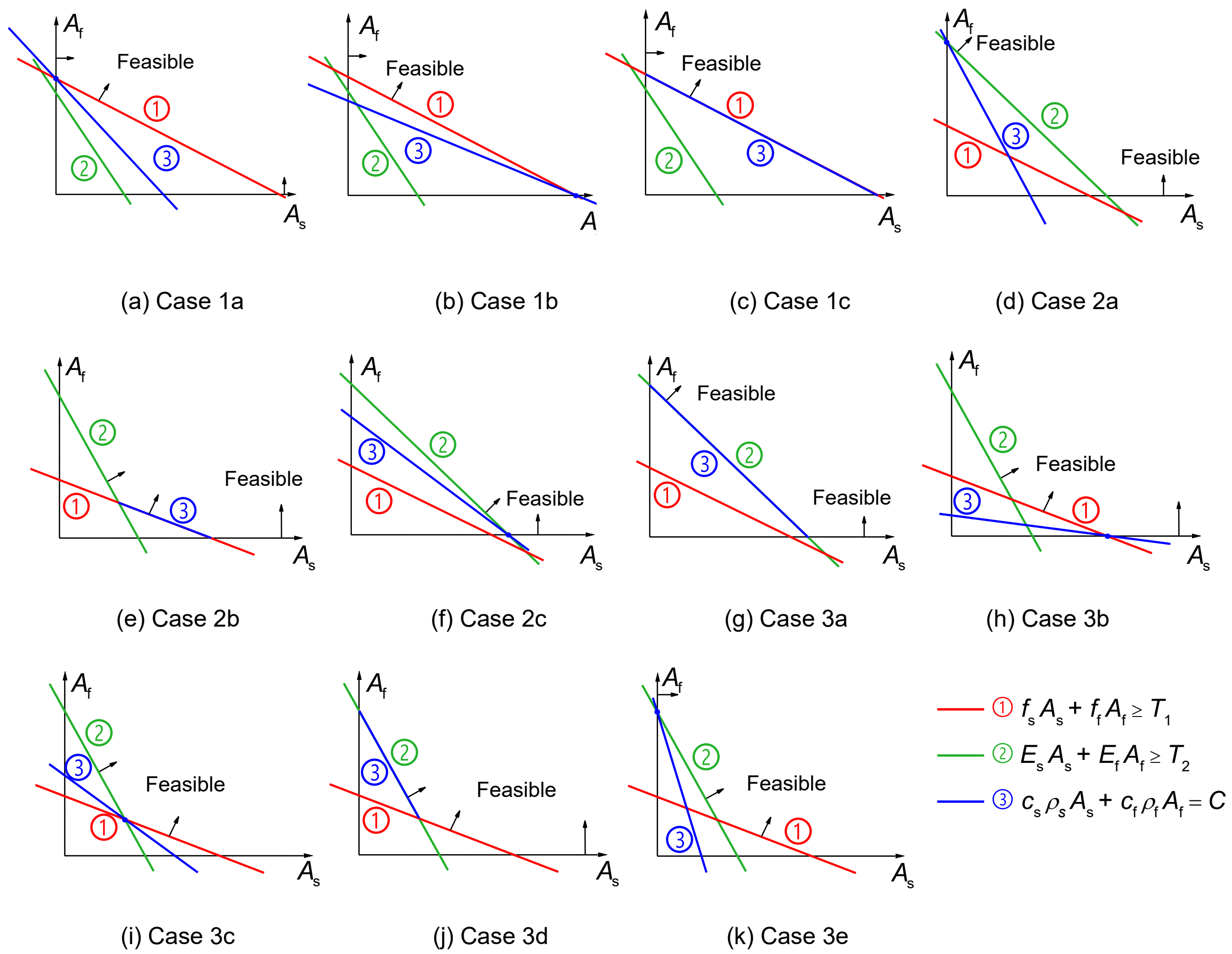

Fig. 3. Different cases of the relative positions of the constraint lines and the corresponding optimal solutions

Table 5. Different cases of the relative positions of the constraint lines and the corresponding optimal solutions (Fig. 3)

Case	Which line shapes the final feasible domain	Slopes $k_1 = -f_s/f_f$ $k_2 = -E_s/E_f$ $k_3 = -c_s\rho_s/(c_f\rho_f)$	Optimal solution for ③	Physical meaning	
1a	① Eq. 3c	$\|k_1\| < \|k_3\|$	$A_s = 0$, $A_f \neq 0$ (Fig. 3a)	The strength criterion always governs the design no matter using steel or BFRP bars	The influence of low f_s/f_f overweighs the influence of low $c_s\rho_s/(c_f\rho_f)$, so steel bars are more carbon efficient for providing strength
1b		$\|k_1\| > \|k_3\|$	$A_s \neq 0$, $A_f = 0$ (Fig. 3b)		The influence of low $c_s\rho_s/(c_f\rho_f)$ overweighs the influence of low f_s/f_f, so BFRP bars are more carbon efficient for providing strength
1c		$\|k_1\| = \|k_3\|$	Any point on ① and on the boundary of the feasible domain (Fig. 3c)		Low $c_s\rho_s/(c_f\rho_f)$ and low f_s/f_f have equal influence, so steel and BFRP bars are equally carbon efficient for providing strength
2a	② Eq. 3d	$\|k_2\| < \|k_3\|$	$A_s = 0$, $A_f \neq 0$ (Fig. 3d)	The stiffness criterion always governs the design no matter using steel or BFRP bars	The influence of high $c_s\rho_s/(c_f\rho_f)$ overweighs the influence of high E_s/E_f, so BFRP bars are more carbon efficient for providing stiffness
2b		$\|k_2\| > \|k_3\|$	$A_s \neq 0$, $A_f = 0$ (Fig. 3e)		The influence of high E_s/E_f overweighs the influence of high $c_s\rho_s/(c_f\rho_f)$, so steel bars are more carbon efficient for providing stiffness
2c		$\|k_2\| = \|k_3\|$	Any point on ② and on the border of the feasible domain (Fig. 3f)		High $c_s\rho_s/(c_f\rho_f)$, and high E_s/E_f have equal influence, so steel and BFRP bars are equally carbon efficient for providing stiffness

Table 5. (Continued)

Case	Which line shapes the final feasible domain	Slopes $k_1 = -f_s/f_f$ $k_2 = -E_s/E_f$ $k_3 = -c_s\rho_s /(c_f\rho_f)$	Optimal solution for ③	Physical meaning	Case
3a		$\lvert k_3 \rvert < \lvert k_1 \rvert < \lvert k_2 \rvert$	$A_s \neq 0$, $Af = 0$ (Fig. 3g)		$c_s\rho_s/(c_f\rho_f)$ is so low that steel bars are more carbon efficient both for providing strength and stiffness
3b		$\lvert k_3 \rvert = \lvert k_1 \rvert < \lvert k_2 \rvert$	Any point on ① and on the boundary of the feasible domain (Fig. 3h)		Steel and BFRP bars are equally carbon efficient for providing strength; as long as the strength requirement is satisfied, the reinforcement quantity automatically satisfies the stiffness requirement
3c	Both ① and ② Eqs. 3c and 3d	$\lvert k_1 \rvert < \lvert k_3 \rvert < \lvert k_2 \rvert$	$A_s \neq 0$, $Af \neq 0$ (Fig. 3i)	When using purely steel bars, the strength criterion governs the design; when using purely BFRP bars, the stiffness criterion governs the design	A combination of steel and BFRP bars is the optimal, as steel bars are more carbon efficient for providing strength and BFRP bars are more efficient for providing stiffness
3d		$\lvert k_1 \rvert < \lvert k_2 \rvert = \lvert k_3 \rvert$)	Any point on ② and on the border of the feasible domain (Fig. 3j)		Steel and BFRP bars are equally carbon efficient for providing stiffness; as long as the stiffness requirement is satisfied, the reinforcement quantity automatically satisfies the strength requirement
3e		$\lvert k_1 \rvert < \lvert k_2 \rvert < \lvert k_3 \rvert$	$A_s = 0$, $Af \neq 0$ (Fig. 3j)		$c_s\rho_s/(c_f\rho_f)$ is so high that BFRP bars are more carbon efficient both for providing strength and stiffness

It is worth noting that the steel-FRP-hybrid reinforcing solution is not yet covered by either ACI 440-1R [1] or the current version of Eurocode 2 [18], despite its demonstrated feasibility in numerous studies [31], [32], [33], [34]. If the hybrid solution is proven optimal (Cases 1c, 2c, 3b, 3c and 3d in Fig. 3) but unviable due to local code compliance or practical constraints, the second-best solution (pure steel or pure BFRP) can also be identified via Fig. 3. In this scenario, the feasible domain contracts to points lying on coordinate axes. Consequently, it is sufficient to compare only two boundary points in the feasible domain: one on the horizontal axis possessing the minimum A_s, and the other on the vertical axis possessing the minimum A_f. The optimal design corresponds to whichever point yields the lower vertical-axis intercept for Eq. 3b.

An example of the section-level comparison using the proposed method is given as follows: for reinforcing a 15-cm-thick concrete flat slab (C25/30) with a 5-meter span, the design of the section should satisfy the ULS criteria under the load combination of 9.4 kN/m^2 and the SLS criterion limiting the deflection to no more than 1/250 of span under the load combination of 4.35 kN/m^2 (obtained by load combinations considering a dead load of 1 kN/m^2, a live load of 2 kN/m^2, and the self-weight); the values in Table 4 for the material properties f_f, f_s, E_f, E_s, c_f, c_s, ρ_f and ρ_s are applied. First, it can be obtained that $|k_1| < |k_3| < |k_2|$. Then, through sectional analysis of the bending-moment resistance, it can be obtained that the strength requirement T_1 = 2.58×10^5 MPa·mm^2; through an estimation of the immediate deflection $\Delta = 5wL^4/(384E_cI_e)$ (w is the uniformly distributed load; L is the span, I_e is the effective moment of inertia of cracked sections), it can be obtained that I_e should be at least 5.71×10^7 mm^4 and T_2 should be at least 4.86×10^7 MPa·mm^2 (it is conservatively assumed that I_e of the mid-span section is used to calculate the deflection of the slab). By drawing the figure with these values, it can be found that the relative positions of the three lines correspond to Case 3c (Fig. 3i). Solving Eqs. 3c and 3d, it can be obtained that A_f = 345.1 mm^2 and A_s = 156.7 mm^2 (corresponding to the intersection point of the lines for Eq. 3c and Eq. 3d, as shown in Fig. 3i) is the optimal solution, which suggests a hybrid reinforcement solution.

5. Carbon efficiency comparison at the structural element level: prismatic elements

Comparison of the carbon efficiency at the structural element level can provide more precise information for the optimal choice of rebar type in terms of reducing the CO_2 of the entire structural element, as the optimal choice of rebar type relies significantly on the structural factors (such as the span and the section depth), and an optimal design, which can achieve the lowest CO_2, is the optimal combination of the all the adjustable factors including the rebar type.

At the structural level, elements can be categorized as either prismatic or non-prismatic. This section compares the carbon efficiency of prismatic elements reinforced with steel or BFRP bars, whilst non-prismatic elements are addressed in Section 6.

It is hypothesised that: a prismatic slab is simply supported under the uniformly distributed loads (dead load G = 1 kN/m^2, live load Q = 2 kN/m^2). The span varies between 3 m and 8 m with step size of 0.1 m. The slab thickness can vary between 0.08 m and 0.32 m with step size of 0.01 m. For each scenario generated by varying the span and the slab thickness, the design is conducted to find the reinforcement quantity using steel bars and BFRP bars, respectively, leading to a steel-reinforced slab and a BFRP-reinforced slab. For simplicity, the design requirements are:

(1) Under the load combination for ULS (1.35G + 1.5Q), the reinforced sections should be able to resist to the bending moment and shear force;

(2) Under the quasi-permanent load combination (G + 0.3Q) for SLS, the long-term deflection should not exceed 1/250 of the span;

(3) The requirement for BFRP-reinforced slabs to avoid creep rupture: the stress in the BFRP bars under the quasi-permanent load combination should not exceed 0.25 of the design tensile strength.

For aspects not specified above, the relevant ACI codes provisions [1], [14] are adopted. The functional unit is defined as a concrete beam reinforced with either steel or BFRP bars that can satisfy the design requirements.

For concrete, the specified compressive strength is 25 MPa and the mean elastic modulus is 31 GPa. For steel bars, the specified yield strength of steel bars is 500 MPa and the elastic modulus is 210 GPa. For BFRP bars, the guaranteed tensile strength is 1200 MPa and the elastic modulus is 50 GPa. The values in Table 4 are taken for the carbon factors and densities.

Fig. 4 shows the design and carbon results of the 15-cm-thick slabs. As shown in Fig. 4a, for BFRP-reinforced slabs, the ULS criteria govern the final reinforcement quantity when the span is shorter than 4.5 m (the "critical span"), whilst SLS criteria govern it for longer spans. In contrast, for steel-reinforced slabs, this switching point happens at a larger value of the span (the critical span of around 5.1 m). When SLS criteria govern the design, for the same span, the required BFRP reinforcement quantity for SLS is always higher than the required steel reinforcement quantity for SLS, which can be explained by the lower elastic modulus of BFRP than that of steel. The final reinforcement quantity is the higher value between the quantity for ULS and that for SLS, and the CO_2 of the final reinforcement are shown in Fig. 4b. In Fig. 4b, the range of CO_2 is obtained using the low and high CO_2 ratios in Table 2 for the lower and upper bounds, respectively. When comparing the slabs reinforced with medium-CO_2 steel bars versus those with medium-CO_2 BFRP bars, when the span is between 4.7 and 5.2 m, the steel-reinforced slabs have lower GWP than their BFRP-reinforced counterparts, whilst BFRP-reinforced slabs have lower GWP when the span is outside this range.

The carbon results of all the slabs (using medium-CO_2 steel bars and medium-CO_2 BFRP bars in Table 2 and ordinary concrete in Table 3) are shown in Fig. 5. It can be observed that, for the slabs of a certain thickness, the pair of curves demonstrates a similar pattern to that of the 15-cm-thick slab in Fig. 4b. When comparing the slabs of different thicknesses at a fixed span, the slab that has the lowest GWP among all slabs (with different thicknesses and types of reinforcement) is always the one reinforced with steel bars, as shown in Fig. 5a. For example, when the span is 5 m, the optimal solution is to use a 15-cm-thick steel-reinforced slab (blue curve in Fig. 5a). The results are presented in three dimensions in Fig. 5b.

This can be explained by Figure 6a which demonstrates the total GWP of the slabs of different thicknesses and reinforcement types when the span is fixed to 5 m. For steel-reinforced slabs, there exists an optimal slab thickness (15 cm) that has the lowest total GWP among all steel-reinforced slabs. When the slab gets thinner than 15 cm, the GWP of the whole slab gets higher because the GWP due to steel reinforcement increases rapidly, as shown in Figure 6b; when the slab gets thicker than 15 cm, more concrete leads to a higher total GWP. Therefore, the optimal solution can maintain a relatively low slab thickness within a certain range (to reduce CO_2 emissions from concrete), while ensuring the thickness is not too low (to prevent a drastic increase in the GWP due to reinforcement). This optimal thickness of 15 cm for the 5-m-span slab corresponds to the point in Fig. 4a that is close to the intersection point of the two curves of steel slabs (at a span between 5.0 m and 5.1 m), which indicates that there is a good balance of ULS and SLS design and the reinforcement quantity is not too much overdesigned for either of them.

For BFRP-reinforced slabs, the shape of the curve in Fig. 6a is similar to that of steel-reinforced slabs but the optimal thickness is larger (17 cm), which can be explained by the lower elastic modulus of BFRP bars. The overall minimum GWP value of the two curves is achieved by the steel-reinforced 15-cm-thick slab, which is coherent with the conclusion drawn from Fig. 5.

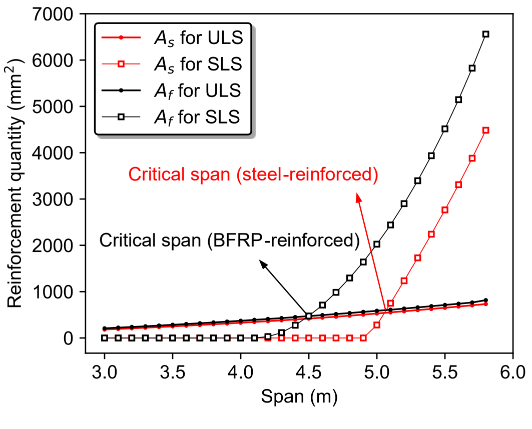

(a)

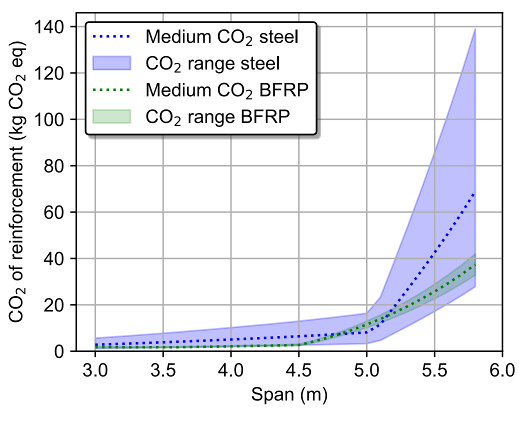

(b)

Fig. 4. Design and carbon results of the 15-cm-thick slabs (a: reinforcement quantities of steel-reinforced slabs and BFRP-reinforced slabs for ULS and SLS, respectively; b: GWP of the reinforcement for steel-reinforced slabs and BFRP-reinforced slabs, respectively)

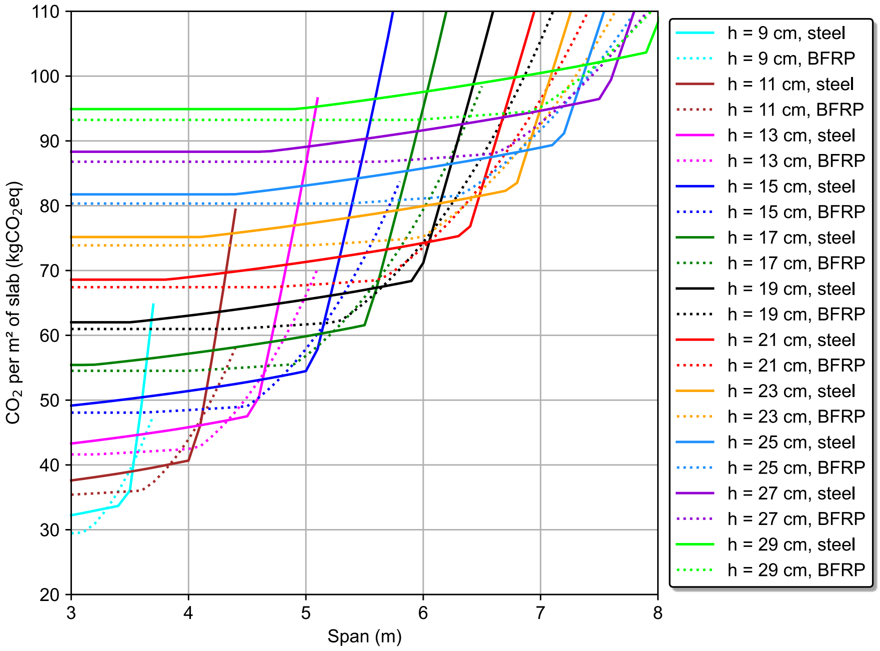

(a)

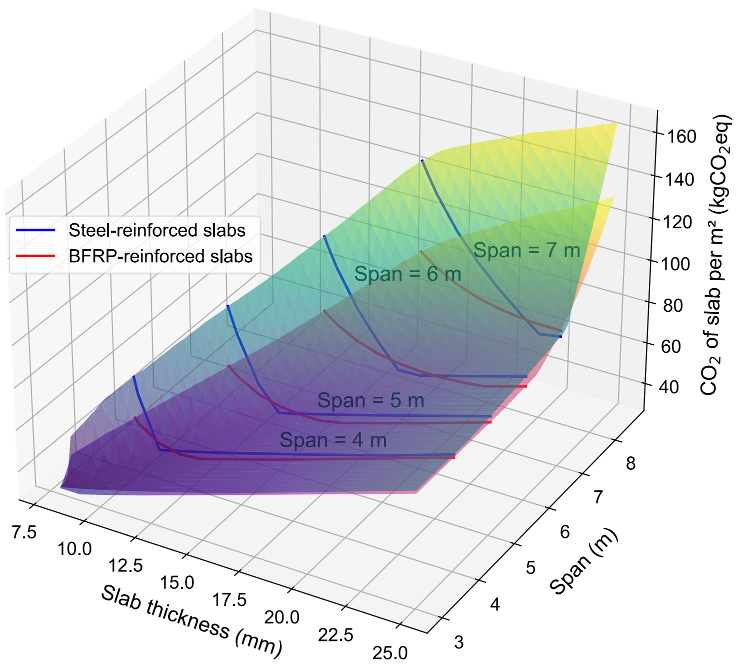

(b)

Fig. 5. GWP of the slabs (total GWP including concrete and reinforcement) reinforced with medium-CO_2 steel bars and medium-CO_2 BFRP bars, respectively, at different spans

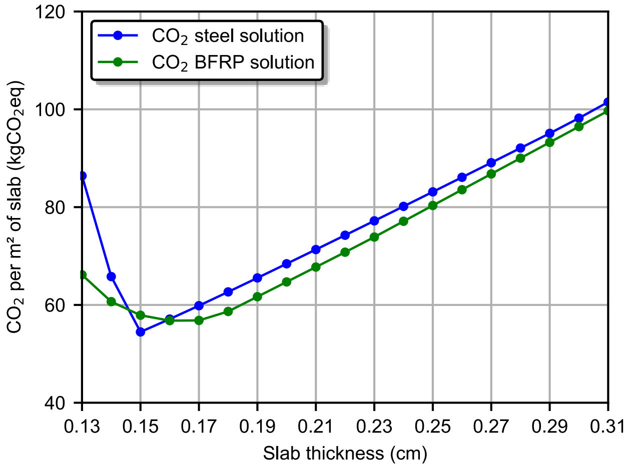

(a)

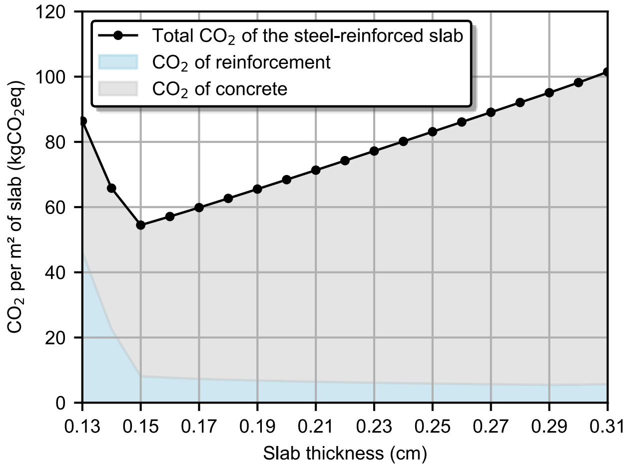

(b)

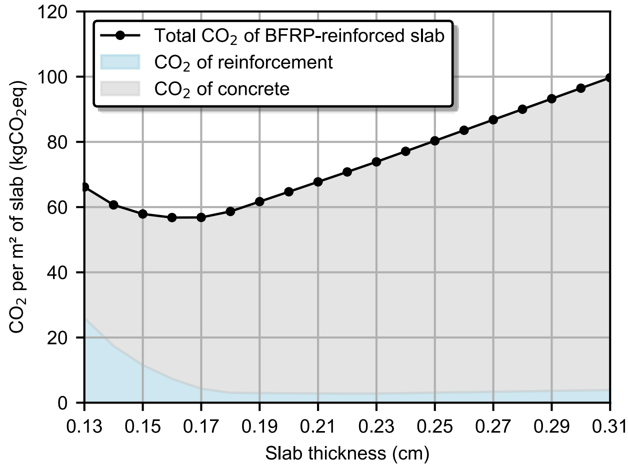

(c)

Fig. 6. GWP of the slabs (including concrete and reinforcement) of different thicknesses and reinforcement types when the span is 5 m (a: GWP of the slabs; b: breakdown of the CO_2 of steel-reinforced slabs; c: breakdown of the CO_2 of BFRP-reinforced slabs)

According to the results of Figs. 4–6, the overall optimal solution is the optimal combination of slab thickness and the reinforcement type. If the span is fixed and the slab thickness is to be freely chosen by structural engineers, steel reinforcement would always be the optimal choice in the presented cases. However, in real construction projects, sometimes the slab thickness is imposed due to other considerations (such as thermal insulation, acoustic insulation and vibration). When there is no freedom for structural engineers to choose the carbon-optimal thickness, the optimal choice of reinforcement type may vary. Fig. 7a shows which of the two reinforcement types is the better choice for achieving a lower overall GWP of the slab when the span and the slab thickness are both fixed. It can be seen that, when the span is given, the steel-reinforced slab can have lower GWP than the BFRP-reinforced slab only when the imposed slab thickness falls within a certain range.

It is important to note that the carbon factors of steel and BFRP bars can have a significant influence on the optimal choice of reinforcement type. As shown in Fig. 7, when the carbon factor of steel reinforcement decreases by 30%, 50% and 60%, the zone where steel reinforcement is optimal becomes larger.

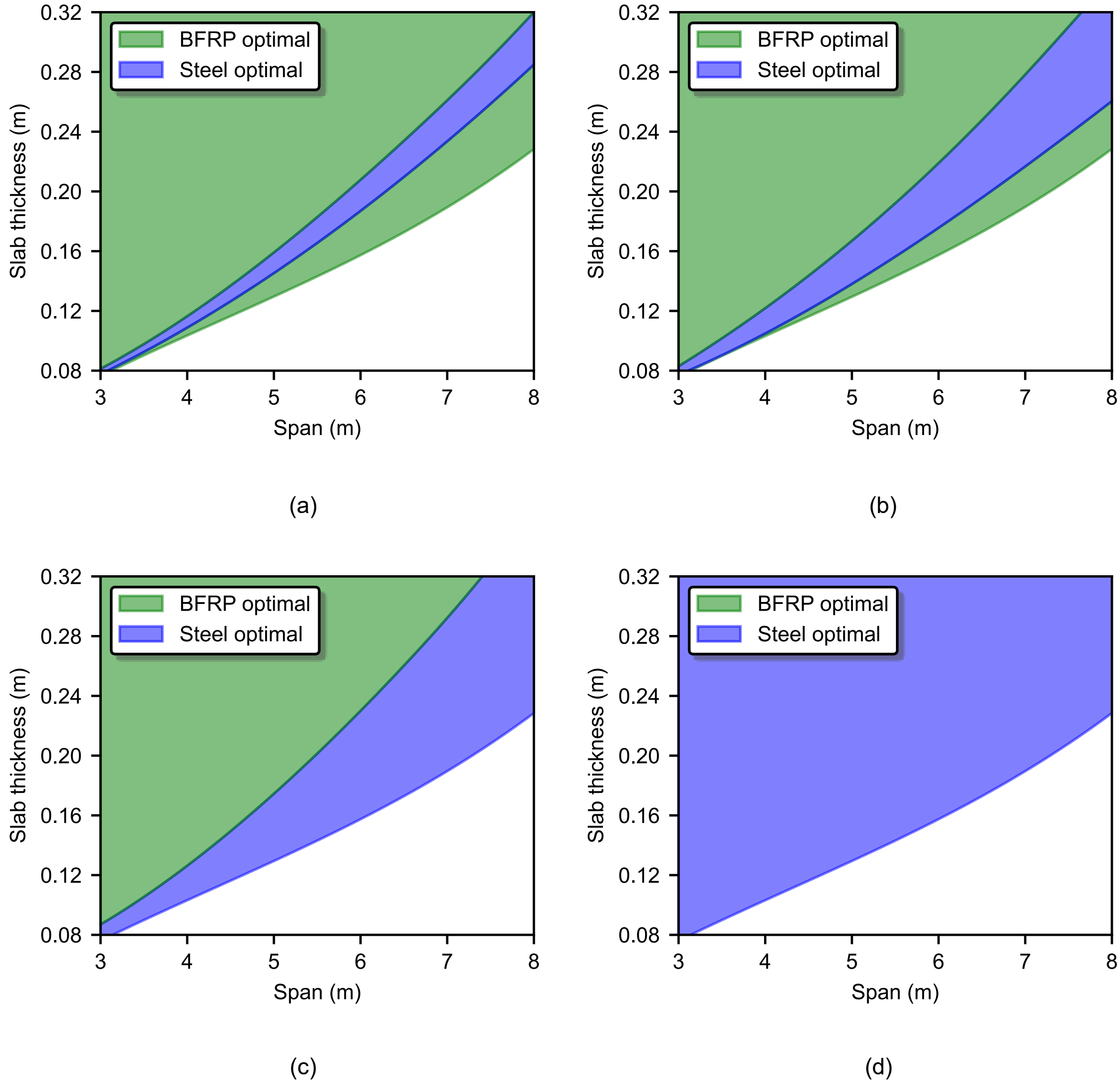

Fig. 7. Optimal choice of reinforcement type between steel bars and BFRP bars to achieve a lower overall GWP of the slab when the span and the slab thickness are fixed (a: medium-CO_2 group in Table 2; b and c: 30% less and 50% less than the medium-CO_2 group; d: low-CO_2 group in Table 2, which is 60% less)

To summarise:

(1) For either steel-reinforced or BFRP-reinforced slabs, when the span is fixed, an overly large thickness leads to high CO_2 from the concrete whilst an overly small thickness leads to high CO_2 from the

reinforcement, both leading to high CO_2 of the whole reinforced slab. An optimal slab thickness exists that can achieve the lowest CO_2 of the whole slab.

(2) For the presented cases with the provided medium carbon factors, when the span is fixed and the thickness is adjustable, the slab with the lowest CO_2 among all steel- and BFRP-reinforced slabs is always the steel-reinforced slab with the optimal thickness for the studied cases.

(3) For the presented cases with the provided medium carbon factors, when the span and the slab thickness are both fixed, the optimal reinforcement type depends on the span and the slab thickness. Steel bars become the optimal choice of reinforcement type only when the slab thickness falls within a certain range; otherwise, BFRP reinforcement is the optimal choice.

(4) Using the same type of bar but with lower CO_2 can totally change the type of the optimal solution.

6. Carbon efficiency comparison at the structural element level: optimised non-prismatic elements

It can be seen from the previous section that the slab thickness plays an important role when choosing the optimal reinforcement. This is because the prismatic slab has a constant thickness along the whole span, and a slight difference in the slab thickness, usually dominated by only one critical section, can lead to a considerable difference in the concrete quantity of the entire element, causing a significant difference in CO_2.

In contrast, for non-prismatic beams and slabs, the local thickness might have a less significant influence on the optimal choice of the reinforcement type, because the thickness varies along the span, and a local increase in the thickness of a certain section does not result in a uniform increase in the concrete quantity across the entire element. As a result, optimised non-prismatic elements could achieve higher carbon efficiency than prismatic elements by using materials only where necessary.

Notably, additional CO_2 emissions may be associated with the formwork necessary for creating curved concrete elements if not carefully managed. Although this aspect falls outside the scope of the present work, such emissions could be reduced using alternative construction methods, such as fabric formwork [35], prefabrication with reusable moulds [36], or 3D printing without formwork [37].

The following example illustrates the methodology and process of comparing the CO_2 emissions of steel- and FRP-reinforced non-prismatic concrete slabs.

It is assumed that a non-prismatic slab is simply supported under the uniformly distributed loads (dead load of 1 kN/m^2, live load of 2 kN/m^2), as shown in Fig. 8. l_2 varies between 3 m and 8 m with step size of 0.1 m, and the ratio l_1/l_2 varies between 0.1 and 0.5. The two types of load distribution should be taken into account, as shown in Fig. 8a, which are the most unfavourable for the zones near the mid-span and near the supports, respectively.

For each combination of l_1 and l_2, two non-prismatic slabs are to be designed, one steel-reinforced and the other BFRP-reinforced, based on the same configuration of shape patterns shown in Fig. 8b; additionally, two reference slabs (prismatic flat slabs, one reinforced with steel and the other with BFRP) are also designed as baselines for CO_2 comparisons.

For the non-prismatic slabs, as shown in Fig. 8b, the lower surface of the slab has two different shape patterns: A and B. For a 1-meter-wide slab, shape patterns A and B account for 30% and 70% of the width, respectively. Shape pattern A is thicker at the mid-span and thinner at the supports, and shape pattern B is the opposite. Shape patterns A and B form the web and flange of a T-section at the mid-span, respectively, whilst near the supports, the roles are reversed, with patterns B and A forming the web and flange. The advantage of this combination of shape patterns, compared to a slab with a single and uniform shape pattern which is thicker both at the mid-span and at the supports, is that there is less risk of concrete spalling or cracking due to the continuous reinforcement through re-entrant corners when the reinforcing bars are straightened.

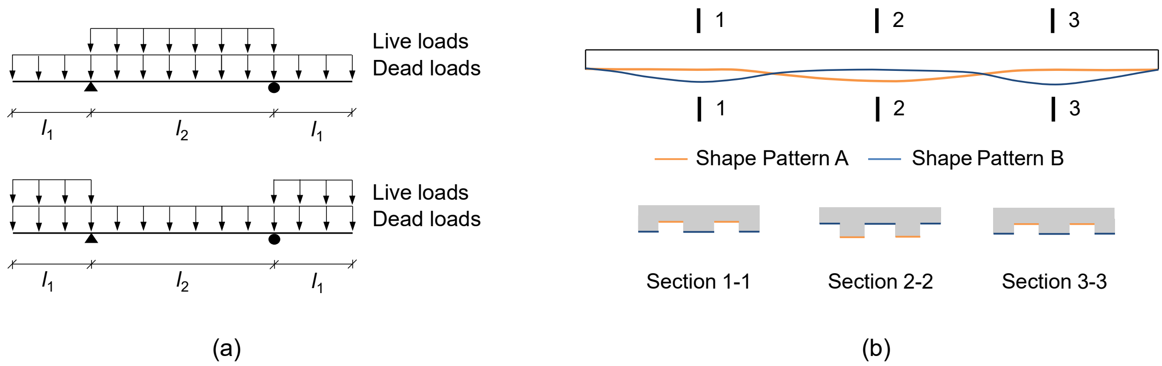

Fig. 8. A simply supported non-prismatic slab (a: the most unfavourable distribution of load for the mid-span section and the section at the supports, respectively; b: the conceptual design of the non-prismatic slab with Shape Patterns A and B alternating in the transverse direction)

For shape pattern A, the reinforcement is on the bottom of the section along the whole slab; for shape pattern B, the reinforcement is on the top of the section and covers the range of $l_1+l_2/3$ at each support. The slab thickness is variable and should not be smaller than 10 cm to ensure sufficient thermal and acoustic insulation performance. In terms of material properties, the same values for concrete, steel bars and BFRP bars as those in Section 5 are used (except that the elastic modulus of BFRP bars is 52.6 GPa). The values of medium-CO_2 steel bars and medium-CO_2 BFRP bars in Table 2 and ordinary concrete in Table 3 are used as the carbon factors. In terms of the design requirements, the same three requirements of Section 5 are taken into account (except for the SLS requirement: the long-term deflection at the mid-span section should not exceed 1/250 of l_2). The functional unit is defined as a concrete beam reinforced with either steel or BFRP bars that can satisfy the design requirements. ACI codes [1], [14] are followed for the design. Other aspects are the same as those in Section 4.

The non-prismatic slabs are designed separately using steel or BFRP bars. For each steel- or BFRP-reinforced slab, the following steps are followed:

- Step 1. The initial size is set for the mid-span section considering the flange thickness (shape pattern B) of 10 cm and the web height (shape pattern A) of l_2/22, and the reinforcement quantity for shape pattern A is obtained by the sectional analysis so that the requirements for the moment resistance as well as the creep rupture of the mid-span section are satisfied for the most unfavourable load distribution (Fig. 8a).
- Step 2. The span is divided into segments of 0.25 m in length. For each section along the entire slab, the reinforcement quantity of shape pattern A obtained in Step 1 is kept constant, and the thickness of shape pattern A at each section along the span of l_2 is obtained through sectional analysis.
- Step 3. The section at the support is designed through sectional analysis considering the flange thickness (shape pattern A) of 10 cm and a reinforcing ratio that is 1.2 times the minimum reinforcing ratio, and the web height (shape pattern B) can be obtained by the sectional analysis so that the requirements for the moment resistance as well as the creep rupture of the section at the support are satisfied for the most unfavourable load distribution (Fig. 8b).
- Step 4. The reinforcement quantity of shape pattern B obtained in Step 3 is kept constant for the zone of l_1+l_2/3, and the thickness of shape pattern B at each section along the span is obtained through sectional analysis.
- Step 5. Through the previous Steps 1-4, the obtained design can satisfy the ULS criteria, but does not necessarily satisfy the SLS criteria. It is checked whether the maximum deflection at the mid-span section is within the allowable value, and if not, the web height (shape pattern A) should be increased iteratively: within each iteration, the most efficient section to increase the thickness for reducing the deflection is identified following the method presented in [38], and a unit concrete thickness of 1 cm is added to the web (shape pattern A) for the identified most efficient section. This process is repeated until the maximum deflection at the mid-span section is no longer excessive, and the final design can satisfy the defined SLS criteria.

The reference slabs are designed using the recommended minimum thicknesses for design suggested by ACI codes [1], [14] (l_2/28 for steel-reinforced slabs and l_2/22 for BFRP-reinforced slabs) as the constant thickness; the quantity of rebar on the bottom of the section is constant for the entire slab and the quantity of rebar on the top of the section is constant over the range of l_1+l_2/3. For simplicity, the transverse reinforcement is not taken into account for any of the slabs, although it would be needed for both non-prismatic slabs and reference slabs in real designs.

Some examples of the designed slabs are shown in Fig. 9, and the comparison of the CO_2 (GWP A1–A3) is shown in Fig. 10.

Comparing the CO_2 of non-prismatic slabs with that of reference slabs, it can be seen that non-prismatic slabs have significantly lower CO_2 than their prismatic counterparts. When comparing the non-prismatic steel-reinforced slabs with prismatic steel-reinforced reference slabs, for the ratio $l_1/\ l_2$ = 0.25 (Fig. 10a), the non-prismatic slabs can achieve CO_2 savings from 4.6% (l_2 = 3 m) to 48.4% (l_2 = 8 m) compared to prismatic slabs, and this range is 6.3%–47.8% and 27.9%–57.5% for the ratio $l_1/\ l_2$ = 0.35 (Fig. 10b) and $l_1/\ l_2$ = 0.45 (Fig. 10c); when comparing the non-prismatic BFRP-reinforced slabs with prismatic BFRP-reinforced reference slabs, the non-prismatic slabs can achieve CO_2 savings of 24.5%–59.1%, 24.3%–60.6% and 54.8%–75.5% compared to prismatic slabs for the ratio $l_1/\ l_2$ of 0.25, 0.35, and 0.45, respectively. This is mainly attributed to shape optimisation which allows using material only where it is necessary, leading to a reduction in material quantity; additionally, the deflection is controlled in an efficient way, without the need to increase the thickness uniformly throughout the entire slab.

Comparing the two groups of prismatic reference slabs, the CO_2 of BFRP-reinforced reference slabs is higher than that of their steel-reinforced counterparts, mainly due to the larger slab thickness and therefore the larger volume of concrete since the recommended minimum thicknesses for design suggested by ACI codes are l_2/28 for steel-reinforced slabs and l_2/22 for BFRP-reinforced slabs for deflection control.

Comparing the two groups of non-prismatic slabs, the difference is not significant: the CO_2 of BFRP-reinforced non-prismatic slabs is slightly lower than that of their steel-reinforced counterparts (6.1%–7.8%, 5.9%–10.6% and 4.8%–14.4% lower for the ratio $l_1/\ l_2$ of 0.25, 0.35, and 0.45, respectively), which is the opposite of the comparison of reference slabs. This can be explained by two reasons: 1) the excessive deflection of BFRP-reinforced slabs due to the lower elastic modulus of BFRP than steel can be addressed by adding more concrete to the most efficient section instead of increasing the thickness uniformly throughout the entire slab; 2) the continuous end of the slab at the supports can mitigate the excessive deflection at the mid-span section, and BFRP-reinforced slabs become more carbon efficient when the design is governed by ULS criteria, similar to Fig. 4a.

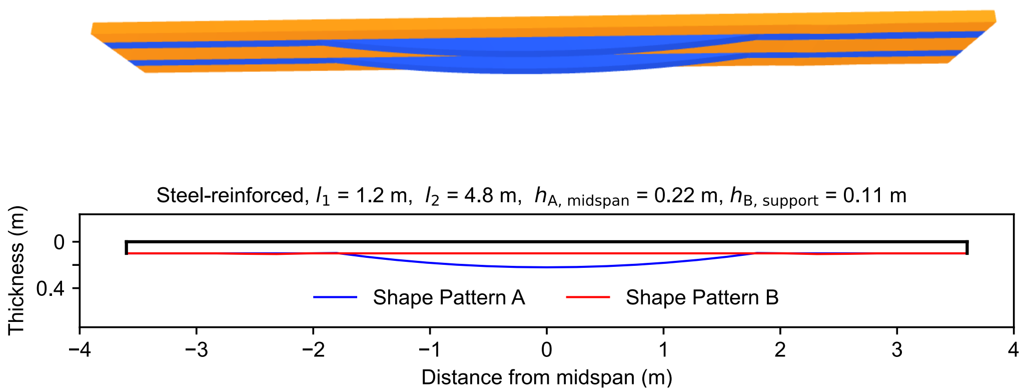

(a)

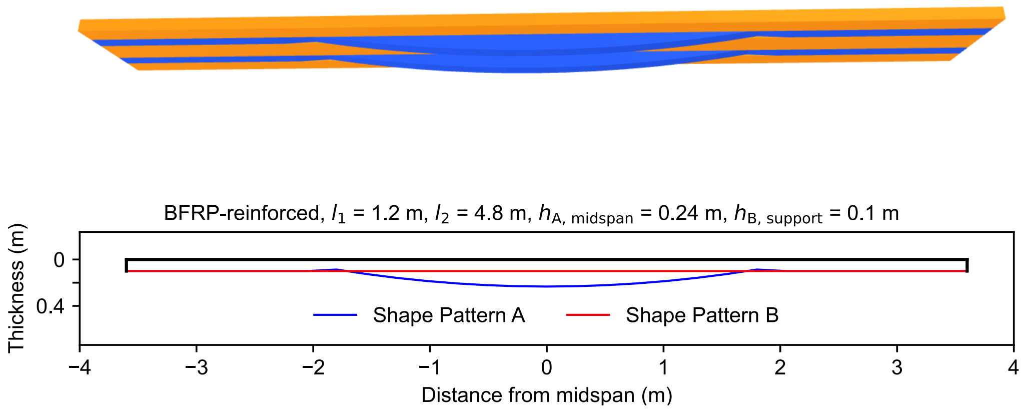

(b)

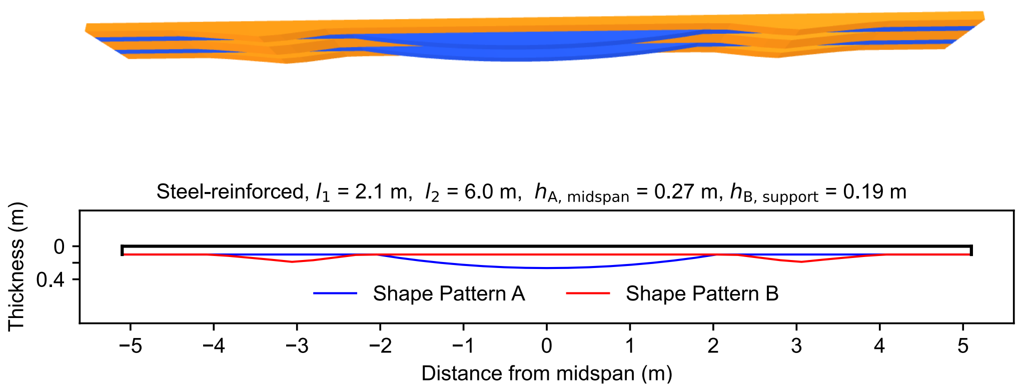

(c)

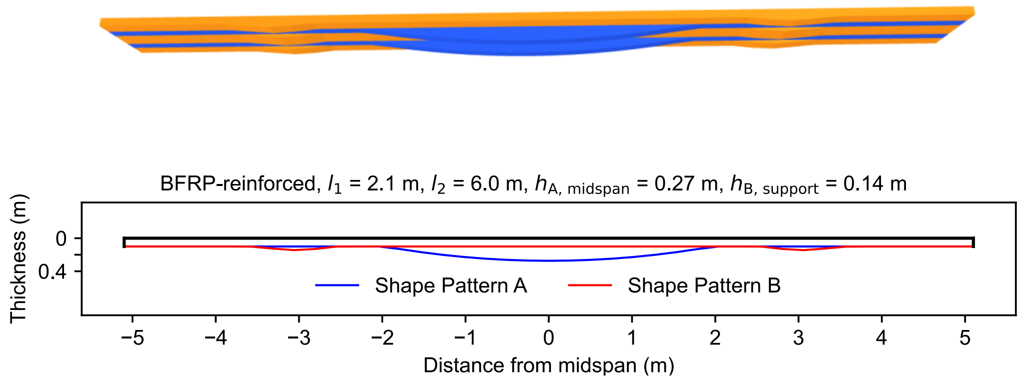

(d)

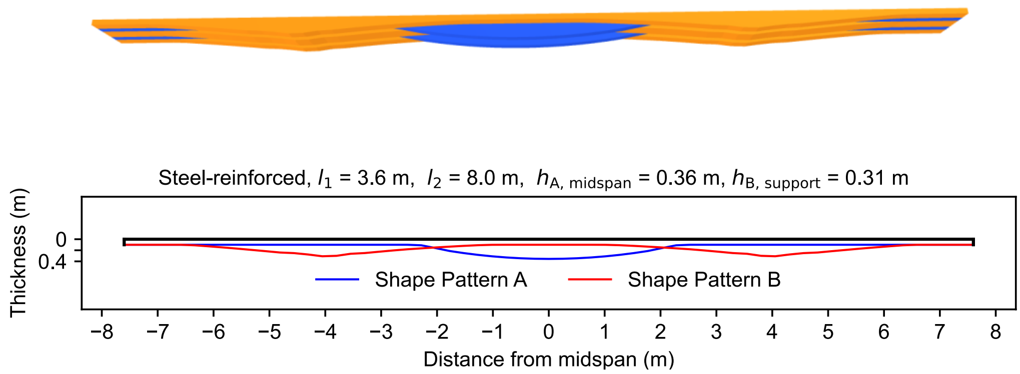

(e)

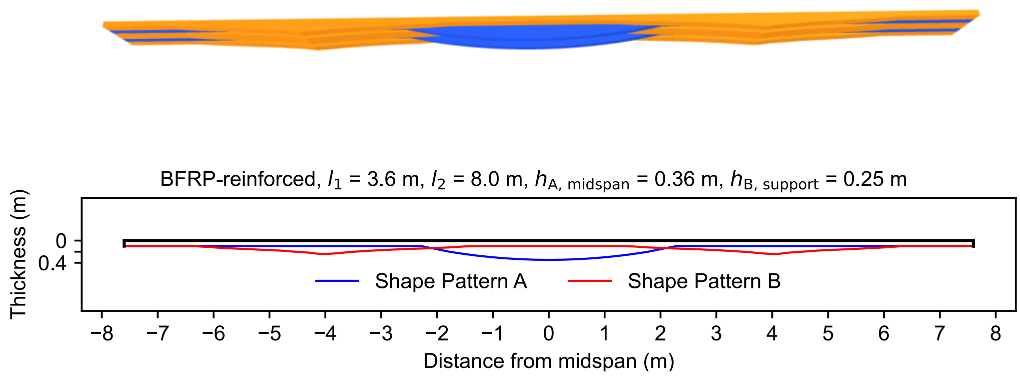

(f)

Fig. 9. Examples of steel- or BFRP-reinforced non-prismatic slab designs (a and b: $l_1/l_2 = 0.25$; c and d: $l_1/l_2 = 0.35$; e and f: $l_1/l_2 = 0.45$)

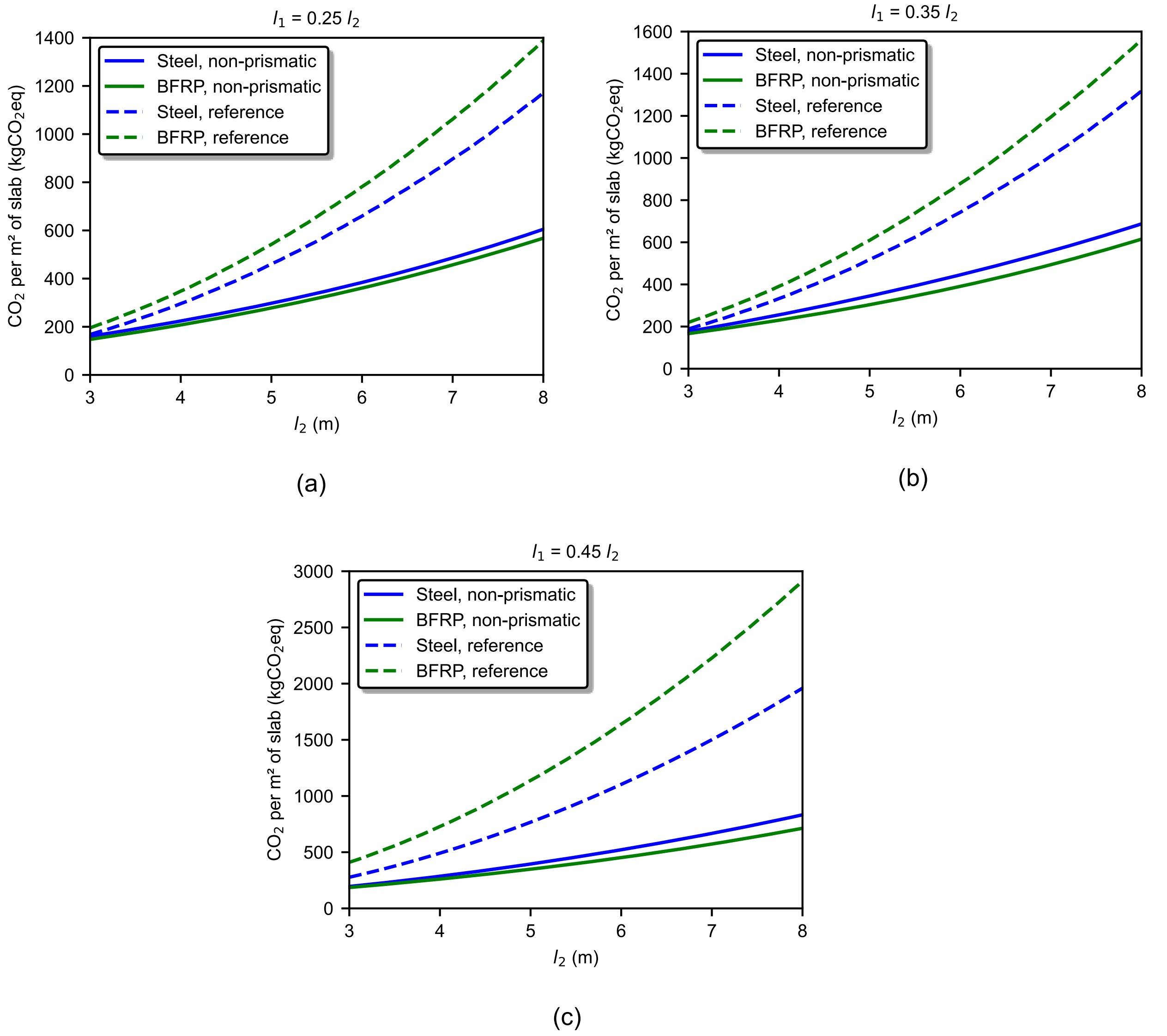

Fig. 10. CO_2 comparison of steel- or BFRP-reinforced non-prismatic and reference slabs (a: $l_1/l_2 = 0.25$; b: $l_1/l_2 = 0.35$; c: $l_1/l_2 = 0.45$)

The overall optimal solution consists of BFRP-reinforced non-prismatic slabs, which achieve CO_2 savings of 12.1%–51.5%, 11.8%–53.4% and 33.1%–63.6% for l_1/l_2 ratios of 0.25, 0.35, and 0.45, respectively, compared to the traditional solution (steel-reinforced prismatic slabs).

To conclude:

(1) By comparing shape-optimised non-prismatic slabs with traditional prismatic slabs with the same type of reinforcement, it can be seen that shape optimisation can achieve significant $CO_{2\ savings}$. When the slab is reinforced with steel bars, shape optimisation can help achieve CO_2 savings of up to 48.4%, 47.8% and 57.5% for the presented example of slabs when the ratio l_1/l_2 is 0.25, 0.35, and 0.45, respectively; when the slab is reinforced with BFRP bars, shape optimisation allows CO_2 savings of up to 59.1%, 60.6%, and 75.5% for the presented example of slabs when the ratio l_1/l_2 is 0.25, 0.35, and 0.45, respectively.

(2) For prismatic slabs, the BFRP-reinforced slabs have higher CO_2 than their steel-reinforced counterparts mainly because ACI codes suggest a greater recommended minimum design thickness for BFRP-reinforced slabs than for steel-reinforced slabs [1], [14].

(3) The overall optimal solution is the BFRP-reinforced non-prismatic slab, which have 4.8%–14.4% lower CO_2 than steel-reinforced non-prismatic slabs, and can save up to 51.5 %, 53.4 % and 63.6 % CO_2 compared to the traditional solution (steel-reinforced prismatic slab) for the ratio $l_1/\ l_2$ of 0.25, 0.35, and 0.45, respectively.

7. Conclusion and discussion

This paper has introduced a comparative framework for multi-level comparisons of the carbon efficiency between FRP and steel bars, from the material-level to the section-level and structural-element-level comparisons, which help provide quantitative comparative results for decision-making when selecting the optimal rebar type for reducing the embodied carbon of structural elements. The applicability of each level of comparison is shown in Table 6.

Table 6. Applicability of carbon efficiency comparisons at different levels

Comparison level	Applicability
Material	Quick comparison at the preliminary design stage, when the carbon data of locally available bars are readily accessible but detailed information about the structural configuration is still unknown
Section	When the sectional-level information is available (the size of section is fixed and the strength and stiffness requirements of the section are known)
Prismatic structural element	When detailed information (such as span and maximum section depth) of a project is available and the structural elements have a constant prismatic section along the span
Non-prismatic structural element	When detailed information (such as span and maximum section depth) of a project is available and the structural elements can be non-prismatic

It is worth noting that these four levels of comparison cannot be considered mutually equivalent since they are based on different hypotheses and each possesses its own limitations. Each level focuses on a distinct scale of analysis, relying on different limited data with varying precision, leading to conclusions that are approximate and applicable only within a specific context or scale. They can be implemented either as standalone evaluations matched to the current project stage and data availability, where only the single most appropriate level of comparison is applied for selecting the optimal reinforcement solution for a construction project; or they can form a sequential and progressive process, with additional levels of comparison conducted as a construction project advances and more structural and environmental data become available, to evaluate the final CO_2 savings following the choice of the reinforcement solution.

The presented examples have demonstrated how each level of comparison should be conducted. The key findings from the presented examples (based on the carbon data of Table 2 and Table 3) are:

- At the material level, steel bars are usually more carbon efficient for providing stiffness whilst BFRP bars are more carbon efficient for providing strength;
- At the section level, the optimal choice of reinforcement type depends on: (1) whether strength or stiffness criteria govern the design of the section; (2) the relative magnitude of CO_2 emissions between steel and BFRP bars.
- At the structural element level (prismatic elements), for either steel-reinforced or BFRP-reinforced slabs, when the span is fixed, there exists an optimal slab thickness that can achieve the lowest CO_2 of the whole slab; with the provided medium group of carbon factors, when the span is fixed but the slab thickness is adjustable, the slab with the lowest CO_2 among all steel- and BFRP-reinforced slabs is always the steel-reinforced slab with the optimal thickness, however, when the span and the slab thickness are both fixed, the steel reinforcement becomes the optimal choice of reinforcement type only when the slab thickness falls within a certain range, otherwise BFRP reinforcement is the better choice.
- At the structural element level (non-prismatic elements), BFRP-reinforced non-prismatic elements have 4.8%–14.4% lower CO_2 than steel-reinforced non-prismatic elements. Regardless of the type of reinforcement, shape optimisation can significantly reduce CO_2 emissions. The most carbon-efficient solution (non-prismatic BFRP-reinforced slabs) can save up to 63% of CO_2 compared to the traditional solution (prismatic steel-reinforced slabs).

The examples are based on the assumption of the carbon data presented in Table 2 and Table 3. Any reduction in the CO_2 emissions of reinforcing bars could substantially alter the comparison outcomes, as it has been shown that the relative CO_2 emission levels between steel and BFRP bars play an important role in assessing their carbon efficiency. For real construction projects, comparisons can be conducted on a case-by-case basis following the introduced comparative multi-level framework and methods using the real project information and updated carbon data.

In terms of the research perspective, it would be interesting to conduct future research in the following aspects:

(1) As the availability of EPD data (particularly for BFRP bars) is limited, further analyses can be conducted in the future when more carbon data become available;

(2) Uncertainty analysis could be useful in the future, as it would provide additional insights to support decision-making;

(3) Comparisons at the structural element level can be conducted with other types of structural elements, such as beams and columns.

References

[1] American Concrete Institute Committee 440, *ACI 440.1R-15: Guide for the design and construction of structural concrete reinforced with Firber-Reinforced Polymer (FRP) bars*. Farmington Hills, MI, US: American Concrete Institute, 2015.

[2] Z. Meghdadi, A. Khaloo, and A. Ashour, "Residual structural performance of fire-exposed concrete slabs reinforced with hybrid GFRP-steel bars: Experimental and numerical studies," *Structures*, vol. 80, no. July, p. 109757, 2025, doi: 10.1016/j.istruc.2025.109757.

[3] X. Wu, X. L. Fan, Z. Y. Xie, M. M. Sun, H. M. Qian, and C. Q. Wang, "Experimental study on punching performance of concrete slab reinforced with GFRP grids," *Structures*, vol. 76, no. April, 2025, doi: 10.1016/j.istruc.2025.108974.

[4] N. F. Grace, A. K. Soliman, G. Abdel-Sayed, and K. R. Saleh, "Behavior and ductility of simple and continuous FRP reinforced beams," *J. Compos. Constr.*, vol. 2, no. 4, pp. 186–194, 1998.

[5] M. R. Maheri and A. Torabi, "Retrofitting external RC beam-column joints of an ordinary MRF through plastic hinge relocation using FRP laminates," *Structures*, vol. 22, no. August, pp. 65–75, 2019, doi: 10.1016/j.istruc.2019.08.004.

[6] A. Confrere, L. Michel, E. Ferrier, and G. Chanvillard, "Experimental behaviour and deflection of low-strength concrete beams reinforced with FRP bars," *Struct. Concr.*, vol. 17, no. 5, pp. 858–874, 2016, doi: 10.1002/suco.201500046.

[7] H. A. Toutanji and M. Saafi, "Flexural behavior of concrete beams reinforced with glass fiber-reinforced polymer (GFRP) bars," *ACI Struct. J.*, vol. 97, no. 5, pp. 712–719, 2000, doi: 10.14359/8806.

[8] B. Kromoser *et al.*, "Article of RILEM TC 292-MCC: life cycle assessment (LCA) of non-metallic reinforcement for reinforcing concrete: manufacturing, durability, dismantling, recycling and reuse: a review," *Mater. Struct. Constr.*, vol. 56, no. 7, pp. 1–24, 2023, doi: 10.1617/s11527-023-02211-y.

[9] N. Stoiber, M. Hammerl, and B. Kromoser, “Cradle-to-gate life cycle assessment of CFRP reinforcement for concrete structures: Calculation basis and exemplary application,” *J. Clean. Prod.*, vol. 280, p. 124300, 2021, doi: 10.1016/j.jclepro.2020.124300.

[10] A. Pavlović, T. Donchev, D. Petkova, and N. Staletović, “Sustainability of alternative reinforcement for concrete structures: Life cycle assessment of basalt FRP bars,” *Constr. Build. Mater.*, vol. 334, p. 127424, 2022, doi: 10.1016/j.conbuildmat.2022.127424.

[11] N. Garg and S. Shrivastava, “Environmental and Economic Comparison of FRP Reinforcements and Steel Reinforcements in Concrete Beams Based on Design Strength Parameter,” in *Proceedings of the UKIERI Concrete Congress*, Jalandhar, India, 2019, pp. 5–8.

[12] P. Khorgade, M. Rettinger, A. Burghartz, and M. Schlaich, “A comparative cradle-to-gate life cycle assessment of carbon fiber-reinforced polymer and steel-reinforced bridges,” *Struct. Concr.*, vol. 24, no. 2, pp. 1737–1750, 2023, doi: 10.1002/suco.202200229.

[13] J. G. Backes, L. Schmidt, J. Bielak, P. Del Rosario, M. Traverso, and M. Claßen, “Comparative Cradle-to-Grave Carbon Footprint of a CFRP-Grid Reinforced Concrete Façade Panel,” *Sustainability*, vol. 15, no. 15, p. 11548, 2023, doi: 10.3390/su151511548.

[14] ACI Committee 318, *Building Code Requirements for Structural Concrete (ACI 318-19)*. American Concrete Institute, 2019. doi: 10.14359/51716937.

[15] V. Brown, “Sustained load deflections in GFRP-reinforced concrete beams,” in *Proceedings of the Third Int. Symposium on Non-Metallic (FRP) Reinforcement for Concrete Structures (FRPRCS-3)*, Sapporo, Japan, 1997, pp. 495–502.

[16] P. Banibayat and A. Patnaik, “Creep Rupture Performance of Basalt Fiber-Reinforced Polymer Bars,” *J. Aerosp. Eng.*, vol. 28, no. 3, 2015, doi: 10.1061/(asce)as.1943-5525.0000391.

[17] French Civil Engineering Association (Association Française de Génie Civil – AFGC), *Utilisation d’armatures composites (à fibres longues et à matrice organique) pour le béton armé – Use of Composite Reinforcement (Long-Fibre and Organic Matrix) for Reinforced Concrete*. Paris, France: AFGC, 2021.

[18] European Committee for Standardization, “EN 1992-1-1:2004 – Eurocode 2: Design of concrete structures – Part 1-1: General rules and rules for buildings,” Brussels, Belgium, 2004.

[19] R. A. Hawileh, F. A. Malhas, and A. Rahman, “Comparison between ACI 318-05 and Eurocode 2 (EC2-94) in flexural concrete design,” *Struct. Eng. Mech.*, vol. 32, no. 6, pp. 705–724, 2009, doi: 10.12989/sem.2009.32.6.705.

[20] M. Inman, E. R. Thorhallsson, and K. Azrague, “A mechanical and environmental assessment and comparison of basalt fibre reinforced polymer (BFRP) rebar and steel rebar in concrete beams,” *Energy Procedia*, vol. 111, no. 1876, pp. 31–40, 2017, doi: 10.1016/j.egypro.2017.03.005.

[21] R. van Gaalen, “Environmental Product Declaration for Basalt Fibre Reinforced Polymer Rebar 6 mm Provided by Galen LLC,” Stichting MRPI®, Amsterdam, Netherlands, 2021. Accessed: May 10, 2026. [Online]. Available: https://www.mrpi.nl/epd-files/epd/1.1.00251.2021_MRPI-EPD_Galen LLC_Basalt Fibre Reinforced Polymer Rebar- 6mm FINAL.pdf

[22] R. van Gaalen, “Environmental Product Declaration for Basalt Fibre Reinforced Polymer Rebar 8 mm Provided by Orlimex CZ,” Stichting MRPI®, Amsterdam, Netherlands, 2022. Accessed: May 10, 2025. [Online]. Available: https://orlitech.co.uk/wp-content/uploads/2023/02/1.1.00388.2022_8mm-MRPI-EPD_Basalt-Fibre-Reinforced-Polymer-Rebar-8mm-_FINAL.pdf

[23] R. van Gaalen, “Environmental Product Declaration for Basalt Fibre Reinforced Polymer Rebar 10 mm Provided by Galen LLC,” Stichting MRPI®, Amsterdam, Netherlands, 2021. Accessed: May 10, 2026. [Online]. Available: https://www.mrpi.nl/epd-files/epd/1.1.00249.2021_MRPI-EPD_Galen LLC_Basalt Fibre Reinforced Polymer Rebar- 10mm FINAL.pdf

[24] O. P. Gibbons and J. J. Orr, *How to calculate Embodied Carbon*. London, UK: The Institution of Structural Engineers, 2020.

[25] EPD Australasia, “Environmental Product Declaration for Reinforcing Bar, Coil and Wire,” EPD Australasia, 2024. Accessed: Oct. 10, 2025. [Online]. Available: https://www.pacificsteel.co.nz/assets/PSL0081-Pacific-Steel-EPD_March-2024-FA_LowRes.pdf

[26] World Steel Association, “Life cycle inventory (LCI) study 2020 data release,” Brussels, Belgium, 2021.

[27] CARES, “Environmental Product Declaration for Carbon Steel Reinforcing Bar,” BRE Global, Watford, UK, 2023.

[28] Global Cement and Concrete Association, “GCCA Policy – Numerical Definitions for Low Carbon and Near Zero Emissions Concrete,” London, UK, 2024.

[29] Holcim UK, “Environmental Projduct Declaration for Concrete C25/30 CIIIA ECOPact produced in plant Aston,” Institut Bauen und Umwelt e.V. (IBU), Berlin, Germany, 2024. Accessed: Oct. 10, 2025. [Online]. Available: https://ibudata.lca-data.com/resource/sources/85479c68-ce64-465a-b46c-88fe796dd211/OriginalEPD.pdf?version=00.01.000

[30] American Society for Testing and Materials (ASTM), *A615/A615M-22: Standard Specification for*

Deformed and Plain Carbon-Steel Bars for Concrete Reinforcement, vol. 1, no. October. West Conshohocken, PA, US: ASTM International, 2010. doi: 10.1520/A0615_A0615M-22.

[31] M. A. Safan, “Flexural behavior and design of steel-GFRP reinforced concrete beams,” *ACI Mater. J.*, vol. 110, no. 6, pp. 677–685, 2013, doi: 10.14359/51686335.

[32] I. F. Kara, A. F. Ashour, and M. A. Köroğlu, “Flexural behavior of hybrid FRP/steel reinforced concrete beams,” *Compos. Struct.*, vol. 129, pp. 111–121, 2015, doi: 10.1016/j.compstruct.2015.03.073.

[33] L. Pang, W. Qu, P. Zhu, and J. Xu, “Design Propositions for Hybrid FRP-Steel Reinforced Concrete Beams,” *J. Compos. Constr.*, vol. 20, no. 4, 2016, doi: 10.1061/(asce)cc.1943-5614.0000654.

[34] F. Peng, J. Deng, and W. Xue, “Design Provisions for Flexural Strength of Hybrid Reinforced Concrete Beams with Fiber-Reinforced Polymer and Steel Bars,” no. 120, pp. 49–60, 2023, doi: 10.14359/51736119.

[35] W. J. Hawkins *et al.*, “Flexible formwork technologies – a state of the art review,” *Struct. Concr.*, vol. 17, no. 6, pp. 911–935, 2016, doi: 10.1002/suco.201600117.

[36] K. S. Elliott, *Precast concrete structures*. Crc Press, 2019.

[37] S. A. Khan, M. Koç, and S. G. Al-Ghamdi, “Sustainability assessment, potentials and challenges of 3D printed concrete structures: A systematic review for built environmental applications,” *J. Clean. Prod.*, vol. 303, p. 127027, 2021, doi: 10.1016/j.jclepro.2021.127027.

[38] S. Hong, J. Orr, and A. Delaplace, “Shape Optimisation of Structural Elements in Flexure for Deflection Control,” in *Proceedings of the 9th World Congress on Civil, Structural, and Environmental Engineering*, London, UK, Apr. 2024. doi: 10.11159/icsect24.139.